Supporting Information

Shields et al. 10.1073/pnas.1005127107

SI Text

As mentioned in the main text, we find a linear relationship between the transport velocity above the cilia tips and the cilia beat frequency, as shown in Fig. S1. The result for the volume flow rate per cilium derived from resistive force theory (Eq. **3**, derived in ref. 1) predicts this linear relationship as well as how the transport rate should scale with the tilted conical beat parameters Θ and Ψ, which is well-matched by our data.

Reynolds Number. The Reynolds number is the ratio of inertial to viscous forces in a fluid medium, typically defined as

$$Re = \frac{\rho u l}{\eta}, \qquad [S1]$$

where ρ and η are the fluid density and viscosity, and u and l are, respectively, characteristic velocity and length scales in the system. To calculate a high-end limit to the Reynolds number in our fluid flows we chose the biomimetic cilium length of 25 μm and the linear velocity of the tip of a cilium beating at 34 Hz. If we assume the cilium tip traces out a circle, then the tip speed is given by $v_{\text{tip}} = \omega L \sin\Psi$, which gives maximum cilium tip speeds up to approximately 1 mm/s. With these characteristic scales the Reynolds number at aqueous viscosities will be $Re = 0.025$. Thus, even at the highest beat frequencies used in our experiments we are still safely in a low Reynolds number environment.

Mixing Enhancement vs. Particle Size. We assume that the cilia-driven advection is size-independent such that D^R_{eff} is constant. Using the maximum relative diffusivity from Fig. 4*B* and obtaining the expected intrinsic diffusivity D^R_0 from the Stokes–Einstein equation, we estimate that the cilia-driven mixing will enhance particle transport as long as $D^R_{\text{eff}} > D^R_0$, which for our data fails to be the case below particle sizes of roughly 10 nm. This is essentially defining an alternative Péclet number as $Pe = D^R_{\text{eff}}/D^R_0$. The minimum particle size for enhanced mixing will be a function of a large number of variables relating to the spatial distribution of cilia and their beat cycle, and so it is difficult to predict this number for the embryonic node. In the context of microfluidic systems, we also expect that the cilia-generated flow field will be independent of the fluid viscosity, assuming that the forced biomimetic cilia motion is unchanged. In this case, the driven mixing would dominate protein diffusion (size ~1 nm) at viscosities larger than 0.01 Pa·s (10 times water).

1. Smith DJ, Blake JR Gaffney EA (2008) Fluid mechanics of nodal flow due to embryonic primary cilia. J R Soc Interface 5:567–573.

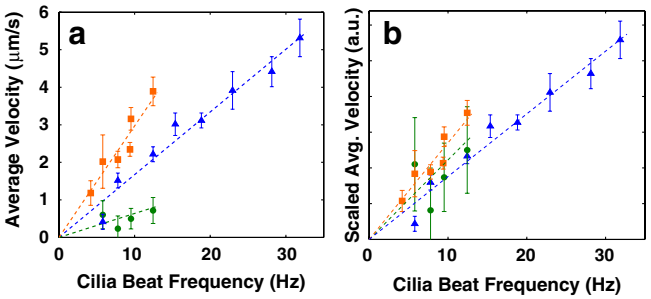

Fig. S1. Average transport velocity vs. cilia beat frequency. (*a*) Average tracer velocity in a plane just above the cilia tips for three different tilted conical beats described by the tilt angle Θ and half-cone angle Ψ, and least-squares linear fits. The fits demonstrate the linear relationship between velocity at the cilia tips and cilia beat frequency. The beat parameters are (•) $\Theta = 24°$, $\Psi = 4.3°$, (▲) $\Theta = 28°$, $\Psi = 7.3°$, and (■) $\Theta = 30°$, $\Psi = 7.8°$. (*b*) Average tracer data from (*a*) scaled by the quantity $\sin^2\Psi \sin\Theta$, which carries the dependence of the pumping rate on the tilted conical beat parameters in Eq. **3**. The collapse of the velocity data to within error bars is consistent with this scaling term explaining the dependence of the transport velocity at the cilia tips on Θ and Ψ.

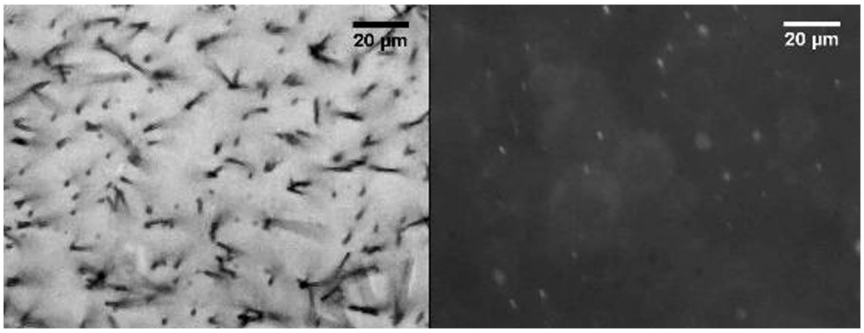

Movie S1. Magnetic actuation of a biomimetic cilia array and directed fluid transport. (*Left*) A brightfield video of the biomimetic cilia mimicking the tilted conical beat of embryonic nodal cilia. The cilia are tilted to the left of the video frame and beating in the clockwise direction, which produces directional fluid transport towards the bottom of the video frame. (*Right*) We observe this directional transport (played at 4× real time) by seeding the fluid with 500-nm fluorescent microspheres that passively trace the fluid motion. The directed transport displayed here is at $z = 30$ μm, which is 5 μm above the tips of the cilia array. Movies were taken with a 50× magnification objective.

Movie S1 (MOV)

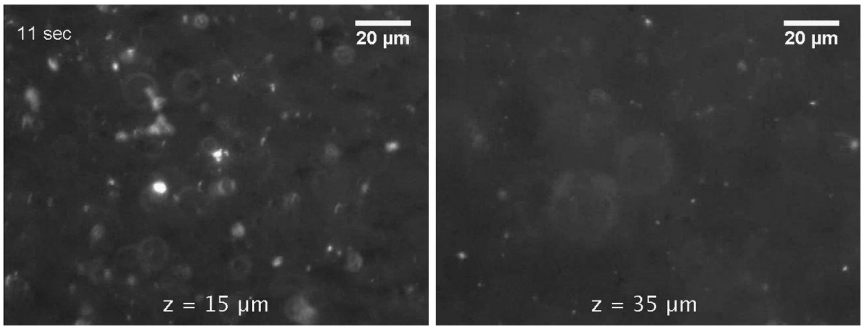

Movie S2. Biomimetic cilia actuation drives two regimes of fluid flow. At left, fluorescent tracer motion below the cilia tips. In this regime, the tracers exhibit rapid velocity fluctuations and little overall directionality. At right, tracer motion above the cilia tips reveals the directed fluid transport analogous to the leftward nodal flow in vertebrate embryos. Both movies are played at 4× real time, and were taken with a 50× magnification objective.

Movie S2 (MOV)

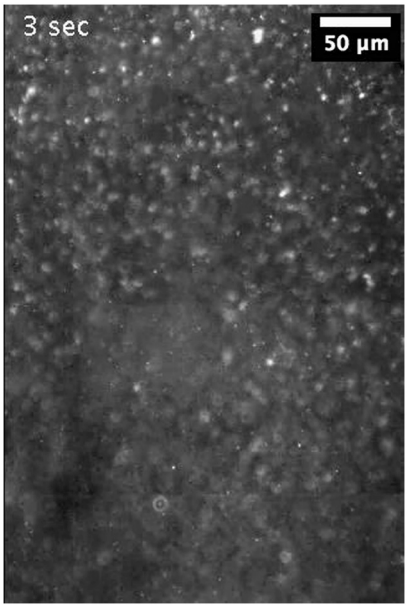

Movie S3. Biomimetic cilia-driven fluid transport at 10× magnification. Three movies taken at 10× magnification were spliced together, allowing us to observe that the directed transport is long-range, persisting across the cilia sample for distances of hundreds of microns. In the center of the movie, a break in the uniformity of the flow is observed that indicates a void of beating cilia in that region. The movie is played at 4× real time.

Movie S3 (MOV)

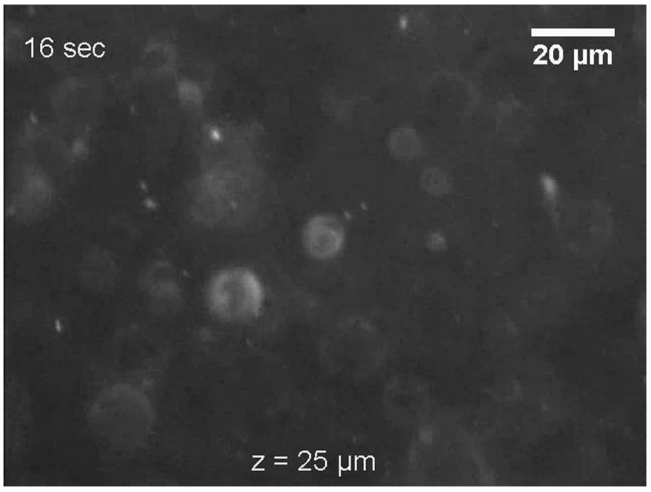

Movie S4. Sequence of movies displaying biomimetic cilia-driven flow at various heights above the sample floor. The tracked tracer data for each movie was used to construct the velocity profile of Fig. 5. The height above the sample floor of each video is indicated at the bottom of the movie frame. The biomimetic cilia tips are at $z = 25$ μm. Below the cilia tips the tracers move with an enhanced diffusivity that increases mixing rates. Near the cilia tips the flow rapidly transitions to the uniform, directed fluid transport. At larger distances from the cilia tips the directed transport slows and eventually changes direction, revealing the recirculation that is a consequence of the enclosed chamber, just as observed in the embryonic node. Movies are played at 8× real time and taken at 50× magnification.

Movie S4 (MOV)